Biology of Reproduction, 2024, 1–15
https://doi.org/10.1093/biolre/ioae055
Research Article

Sertoli cells require hnRNPC to support normal spermatogenesis and male fertility in mice†

Shaomei Mo[1,‡], Ge Shu[1,‡], Congcong Cao[1], Mingxia Wang[1], Jie Yang[1], Jing Ye[1], Yaoting Gui[1,*], Shuiqiao Yuan[2,3,*] and Qian Ma[1,4,*]

[1]Shenzhen Key Laboratory of Male Reproductive Medicine and Genetics, Department of Urology, Peking University Shenzhen Hospital, the Fifth Clinical College of Anhui Medical University, Shenzhen, Guangdong, China
[2]Institute of Reproductive Health, Tongji Medical College, Huazhong University of Science and Technology, Wuhan, China
[3]Laboratory Animal Center, Huazhong University of Science and Technology, Wuhan, Hubei, China
[4]Institute of Urology, Shenzhen PKU-HKUST Medical Center, Shenzhen, Guangdong, China

***Correspondence:** Institute of Reproductive Health, Tongji Medical College, Huazhong University of Science and Technology, Wuhan, China. E-mail: shuiqiaoyuan@hust.edu.cn; Institute of Urology, Shenzhen PKU-HKUST Medical Center, Shenzhen, Guangdong, China. E-mail: mq@whu.edu.cn; Shenzhen Key Laboratory of Male Reproductive Medicine and Genetics, Department of Urology, Peking University Shenzhen Hospital, Shenzhen, Guangdong 518036, China. Tel: +8675583923333; Fax: +8675583923333; E-mail: guiyaoting2023@aliyun.com

†**Grant Support:** This work was supported by grants from the National Natural Science Foundation of China (grant numbers 82001559 and 82171605), Guangdong Foundation of Basic and Applied Basic Research (grant number 2019A1515110884), Shenzhen High-level Hospital Construction Fund (grant number YBH2019-260), and Medical Scientific Research Foundation of Guangdong Province (grant number A2022427).
‡Shaomei Mo and Ge Shu contributed to this work and share first authorship.

Abstract

Sertoli cells act as highly polarized testicular cells that nutritionally support multiple stages of germ cell development. However, the gene regulation network in Sertoli cells for modulating germ cell development has yet to be fully understood. In this study, we report that heterogeneous nuclear ribonucleoproteins C in Sertoli cells are essential for germ cell development and male fertility. Conditional knockout of heterogeneous nuclear ribonucleoprotein C in mouse Sertoli cells leads to aberrant Sertoli cells proliferation, disrupted cytoskeleton of Sertoli cells, and compromised blood–testis barrier function, resulting in loss of supportive cell function and, ultimately, defective spermiogenesis in mice. Further ribonucleic acid-sequencing analyses revealed these phenotypes are likely caused by the dysregulated genes in heterogeneous nuclear ribonucleoprotein C–deficient Sertoli cells related to cell adhesion, cell proliferation, and apoptotic process. In conclusion, this study demonstrates that heterogeneous nuclear ribonucleoprotein C plays a critical role in Sertoli cells for maintaining the function of Sertoli cells and sustaining steady-state spermatogenesis in mice.

Graphical Abstract

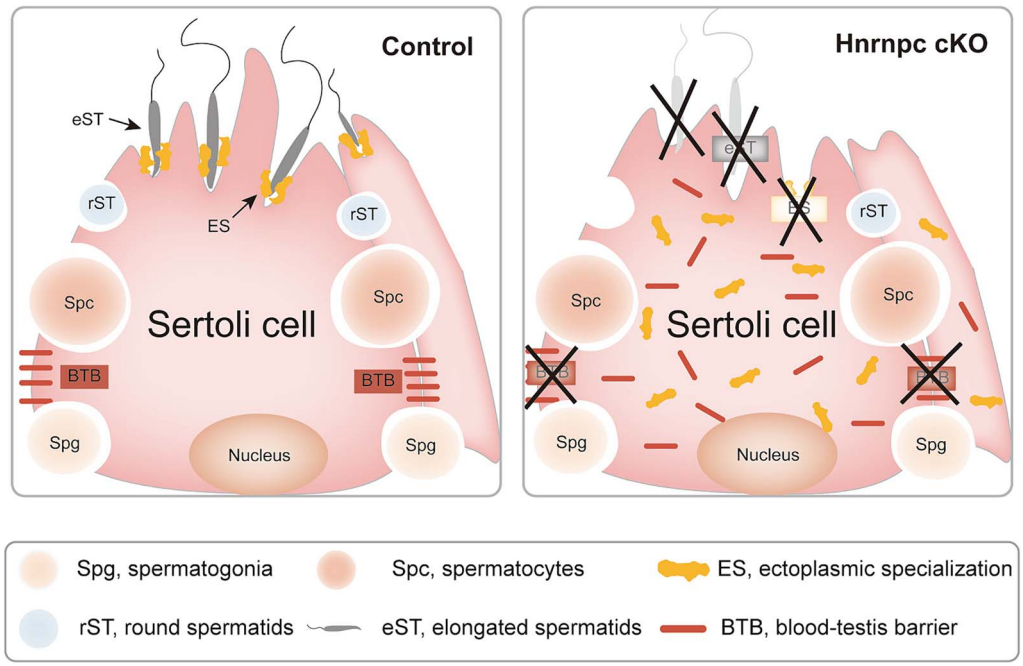

Key words: hnRNPC, blood–testis barrier, Sertoli cells, spermatogenesis, testis

Received: May 30, 2023. **Revised:** October 17, 2023. **Accepted:** April 1, 2024

Introduction

Spermatogenesis is a complex process that is behind the production of sperm from the primordial germ cells (GCs) and consists of the mitosis of spermatogonia (SPG), meiosis of spermatocyte, and spermiogenesis [1, 2]. Defects in any of the steps might result in male infertility [3]. Sertoli cells (SCs) are the most critical somatic constituent of the testicular seminiferous epithelium and play a crucial role during spermatogenesis by providing nutrients to support the growth of GCs. Both SCs and GCs in the testis are organized in a highly polarized manner to support spermatogenesis, such as by accommodating the maximum number of GCs in the limited space of the seminiferous epithelium [4]. The adjacent SCs could form a blood–testis barrier (BTB) that divides the seminiferous epithelium into the basal and the apical compartments. Structurally, the BTB is composed of the tight junction (TJ) [5, 6], the basal ectoplasmic specialization (ES) [7], and the gap junction (GA) [8, 9]. Therefore, the integrity of BTB, including proper basal–apical ES localization, is essential for spermatogenesis.

Recent studies have highlighted the importance of specific metabolic pathways in SCs [e.g., mammalian target of rapamycin complex 1 (mTORC1) and AMP-activated protein kinase (AMPK) pathways] due to their function in regulating SC metabolism and energy balance to support GC development and differentiation. Dysregulation of these pathway-related genes can lead to male infertility or subfertility in mice, as seen in mouse models with conditional knockout of mTOR or AMPK catalytic subunit $\alpha 1$ in SCs [10, 11]. Overall, the proper functioning of signal pathways and gene regulatory networks in SCs is essential for the maintenance of spermatogenesis, and their roles extend beyond nutritional support. Therefore, investigating the molecular mechanisms of gene regulation in SCs is a step toward better understanding male infertility and developing potential treatments.

Heterogeneous nuclear ribonucleoproteins (hnRNPs) are ribonucleic acid (RNA)–binding proteins that participate in the regulation of various aspects of cellular RNA metabolism, such as alternative splicing [12], nuclear retention and export [13], stability [14], and translation of messenger RNA (mRNA) [15]. Many members of the hnRNP family of proteins have been reported to be expressed in the testes and have essential roles in spermatogenesis, including heterogeneous nuclear ribonucleoprotein G-T, heterogeneous nuclear ribonucleoprotein L, heterogeneous nuclear ribonucleoprotein K, Heterogeneous nuclear ribonucleoprotein U (hnRNPU), heterogeneous nuclear ribonucleoprotein H1 (hnRNPH1), and heterogeneous nuclear ribonucleoproteins A2/B1 [16–22], but there is still a lack of research on the relationship between hnRNPC and spermatogenesis. Specifically, we previously found that the proliferation capacity of SCs and GCs was dramatically decreased due to male sterility in deficiency of hnRNPU in murine SCs [19] and depletion of *Hnrnph1* in SCs results in abnormal splicing events associated with meiotic processes and crosstalk between GCs–SCs [23]. Heterogeneous nuclear ribonucleoproteins C has two isoforms, hnRNC1 and hnRNPC2, genetically encoded by a single gene and produced by alternative splicing of the same transcript [24, 25]. Previous studies showed that the expression of the hnRNPC was upregulated in multiple tumors or tumor cell lines, such as pancreatic cancer [26], hepatocellular carcinoma [27], and breast cancer [28]. However, the function of hnRNPC in SCs has never been evaluated, as global knockout of *Hnrnpc* leads to embryonic death at embryonic day 10.5 (E10.5) [29], prior to the establishment of the SC population.

In this study, we created an SC–specific knockout *Hnrnpc* mouse model (*Hnrnpc* cKO) and found that the proliferation of immature SCs was significantly decreased upon hnRNPC depletion in SCs, which caused a reduction in the number of both SCs and GCs. The expression patterns of cytoskeleton proteins, as well as junction proteins, were also altered, which led to the disruption of BTB integrity in testes and, ultimately, male sterility in *Hnrnpc* cKO mice. At molecular levels, we found that many genes related to cell adhesion, cell proliferation, and apoptotic process were deregulated in hnRNPC-deficient SCs. Collectively, these results reveal that hnRNPC in SCs is critical for the maintenance of SC function and GC development.

Materials and methods

Animals

All animal experiments in this study were performed in specific-pathogen-free laboratory rooms and conducted in accordance with the guidelines published by the Institute of Laboratory Animal Resources for the National Research Council. The study was approved by the ethics committee of Peking University Shenzhen Hospital and the animal center of Shenzhen PKU-HKUST Medical Center (approval number: 2022-1011).

All mice used in this study are C57BL/6 J background. The floxed *Hnrnpc* transgenic mice were created using the clustered regularly interspaced short palindromic repeats (CRISPR)/CRISPR associated protein 9 strategy from GemPharmatech Company (Nanjing, China), and the *Amh-Cre* deletor mice were acquired from Jackson Laboratory. *Amh-Cre; Hnrnpc*$^{flox/+}$ mice were generated by crossing *Amh-Cre* males with *Hnrnpc*$^{flox/flox}$ females. Then, the *Amh-Cre; Hnrnpc*$^{flox/+}$ were subsequently bred with *Hnrnpc*$^{flox/flox}$ mice to produce *Amh-Cre; Hnrnpc*$^{flox/flox}$ (designated as *Hnrnpc* cKO or cKO) males. We used *Amh-Cre; Hnrnpc*$^{flox/+}$ mice or *Hnrnpc*$^{flox/flox}$ mice as control (Ctrl) mice for histological analysis and C57BL/6 J wild-type (WT) mice as Ctrl mice for RNA sequencing (RNA-seq) analysis, respectively, in this study. It usually takes about 6 months to obtain the cKO mice, which are bred for about three generations before being obtained. Genotyping of the mice was performed using genomic deoxyribonucleic acid (DNA) extracted from the mouse tail by a polymerase chain reaction (PCR)–based method. PCR cycling conditions were used as follows: initial denaturation at 95°C for 5 min, followed by 35 cycles of 95°C for 30 s, 60°C for 30 s, and 72°C for 30 s; then, 72°C for 5 min and kept at 4°C before detection. The sequences of primers are presented in Supplementary Table S1.

Fertility test

To assess fertility, each adult WT or *Hnrnpc* cKO male mice ($n = 6$ for each genotype) were matched with two random adult WT fertility–proved females for at least four months, respectively. WT female mice were obtained from the GemPharmatech Company (Nanjing, China). Cages were monitored daily, and litter and pup counts were recorded.

Sperm counting

The cauda epididymes were dissected, minced, and incubated in Quinn's Advantage Fertilization human tubal fluid (HTF) Medium (ART-1020, SAGEIn-VitroFertilization, USA) medium for 15 min at 37°C. A small amount of the sperm suspension was diluted in HTF medium to determine the sperm concentration. The diluted sample was then loaded onto a Macro sperm counting chamber, a special type of microscope slide with a grid pattern etched onto its surface. Then the sperm number and motility was assessed by CASA system. To calculate the sperm counts more accurately, we also counted the sperm number manually. Briefly, the number of sperm within the grid was counted under a light microscope at ×10 magnification, and the total sperm count in the original sample was calculated using the following formula: sperm concentration = (number of sperm counted/volume of diluted sample) × dilution factor.

Histology and immunohistochemistry

The testis and epididymis of mice were fixed in Bouin's solution (HT10132, Sigma-Aldrich, USA) at room temperature (RT) for 18–20 h or 4% paraformaldehyde (PFA) overnight at 4°C. Then, the specimens were embedded in paraffin for further histological evaluation. Periodic Acid Schiff (PAS) staining was performed on microsections with 5 μm of thickness using a kit (G1281, Solarbio, China). Briefly, the sections were deparaffinized in xylene, rehydrated from ethanol to water, and then stained with PAS, followed by counterstaining with hematoxylin. For immunohistochemistry (IHC), the sections were submerged entirely into 0.01 M citrate buffer (G1205, Servicebio, Wuhan, China) in a microwave for antigen retrieval and cooled at RT for 2–3 h after routine dewaxing and hydration. The sections were then washed three times with phosphate-buffered saline (PBS) (5 min each time) and incubated with 3% hydrogen peroxide at RT for 15 min. After blocking in 5% bovine serum albumin (BSA) (V900933, Sigma-Aldrich, USA) for 1 h, the sections were incubated in a dark environment with primary antibodies and kept at 4°C overnight. Sections were then washed in PBS for three times (10 min each) and incubated with secondary antibodies at RT for 1 h. After washing with PBS and colored with DAB substrate kit (DAB-0031, MXB Biotechnologies, China) at RT, the sections were stained with hematoxylin for 2 min and washed with double distilled water. Subsequently, sections were dehydrated in gradient alcohol, transparent in xylene, and sealed with neutral gum. Then images were captured under white light using the microscope (Olympus, BX53, Tokyo, Japan). The details of all commercial antibodies used in this study are presented in Supplementary Table S2.

Immunofluorescence staining

For immunofluorescence (IF) staining, testes were fixed in 4% PFA overnight at 4°C and then treated with gradient sucrose and embedded in optimal cutting temperature compound (OCT, 4583, Sakura Finetek, USA) medium (50% OCT plus 50% sucrose). The testis samples were cut into 5 μm-thick sections and then immersed in 0.01 M citrate buffer and microwaved for 20 min for antigen retrieval. Nonspecific binding was blocked with a 5% BSA blocking solution for 1 h at RT. The sections were incubated with the primary antibodies overnight at 4°C in a dark environment and then incubated with secondary antibodies for 1 h at RT. After washing with PBS and stained with VECTASHIELD antifade mounting medium containing 4′,6-diamidino-2-phenylindole (DAPI) (H-1200-10, Vectorlabs, USA), the sections were photographed under a confocal microscope (STELLARIS 5, Leica, Germany). The positive cells [Wilms tumor 1 (WT1), 5-Ethynyl-2′-deoxyuridine (EdU), apoptosis] in each tubule on the slide were counted, and at least three nonconstitutive sections from each mouse were detected. Over 100 tubules from testicular sections from three biological replicates were analyzed for positive cell counts. The antibodies used in this study are presented in Supplementary Table S2.

Western blot

Protein was extracted from mouse testes or purified SCs using radioimmunoprecipitation assay lysis buffer (WB3100, NCM Biotech, China) and quantified by BCA (Bicin-choninic Acid) protein assay kit (23227, Thermo Scientific, USA) according to the manufacturers' instructions. Then equal amounts of protein (30 μg of each sample) were separated by 10% sodium dodecyl-sulfate polyacrylamide gel electrophoresis. Protein in gels was then transferred to the polyvinylidene fluoride (PVDF) membranes (0.22 μm, Millipore, USA) through the wet-transfer method. Subsequently, the PVDF membranes were blocked with 5% nonfat milk diluted in Tris-buffered saline containing Tween-20 [TBST, 10 mM Tris–HCl, 150 mM NaCl, 0.05%(V/V) Tween-20] at RT for 1 h on a shaker (80 rpm/min) and incubated with the primary antibodies diluted in 5% nonfat milk overnight at 4°C in a wet chamber. The membranes were then washed three times (10 min each) with TBST and incubated with HRP Goat Anti-Mouse IgG (AS003, ABclonal, China) or Anti-rabbit IgG HRP-linked antibody (7074, Cell Signaling Technology, USA). The signals were detected using an ECL Chemiluminescence Kit (WBKLS0500, EMD Millipore, USA).

Real-time polymerase chain reaction analysis of target genes

Total RNAs were extracted from testes or SCs using TRIzol reagent (15596026, Invitrogen, USA), and the concentration was quantified using a Nanodrop ND-2000 spectrophotometer (Thermo Scientific). Complementary DNA (cDNA) was synthesized from 1 μg or 0.5 μg total RNA with Hiscript II 1st Strand cDNA Synthesis Kit (R211, Vazyme, Nanjing, China) following the manufacturer's instructions. Real-time polymerase chain reaction (RT-qPCR) was performed using Cham Q SYBR qPCR Master Mix (Q711–02, Vazyme, Nanjing, China) according to the official instructions, and then analyzed by Roche LightCycler 480 Instrument II. *Gapdh* was used as endogenous Ctrl. The primers used for RT-qPCR were listed in Supplementary Table S1.

5-Ethynyl-2′-deoxyuridine staining

EdU staining was conducted using the BeyoClick EdU Cell Proliferation Kit (C0075L, Beyotime, China). Briefly, the cultured primary SCs isolated from testes were incubated with EdU (10 nM) for 24 h and then fixed with 4% PFA at RT for 15–20 min. After permeabilizing the cells in 24-well plates with 0.3% Triton X-100 for 15 min, the cells were incubated with click reaction solution for approximately 30 min and then stained with DAPI. A confocal microscope (Zeiss 510, Germany) was used to capture the images. Numbers of positive cells were quantified was carried out using ImageJ software (Version 5.0, USA).

Primary Sertoli cell isolation

The testes of WT and *Hnrnpc* cKO mice at P3, P5, P14, and P56 were softly removed and decapsulated in Hanks Balanced Salt Solution (HBSS, 14170112, Gibco) for SCs isolation as described previously [30]. Briefly, the testicular tissue samples were placed in a 50 ml sterile centrifuge tube prepared by adding 10 ml Dulbecco Modified Eagle Medium (DMEM)/F12 medium (11320033, Gibco) with 0.5 mg/ml deoxyribonuclease I (DN25-100 mg, Sigma), 0.5 mg/ml hyaluronidase (H3506-100 MG, Sigma), and 1 mg/ml collagenase IV (C5138-100 mg, Sigma). After digestion (37°C, 10 min, using a shaker), the seminiferous tubules were allowed to settle before being washed twice with DMEM/F12 medium. The solution was then treated with 2.5 mg/ml trypsin (25200072, Gibco) and 0.5 mg/ml deoxyribonuclease I for approximately 30 min at 37°C. Afterward, the digestion was immediately stopped by adding 10% FBS and filtering through a 40 μm nylon mesh to prepare a single-cell suspension. The filtered suspensions were centrifuged at 600 g for 5 min and cultured in a 60 mm dish or 24-well plates at 35°C with 5% carbon dioxide for 48 h. To remove male GCs and other types of cells, cells were washed once with HBSS, incubated with hypotonic shock solution (20 mM Tris–HCl, PH = 7.4, in distilled water) for 3 min, followed by two washes of HBSS. After the treatment, cells were cultured for 24 h and then prepared for further experiments. Freshly purify of isolated primary SCs were assessed by immunostaining with antibodies against WT1, as well as RT-qPCR analysis for *Sox9* (SC marker) and *Cyp17a1* (Leydig cell marker). *Gapdh* was used as Ctrl. Compared with *Sox9*, the mRNA expression of *Cyp17a1* could be barely detected, which combined with antibody staining, proved a more than 95% purity of SCs isolated.

Biotin tracer assay

The blood–testis barrier permeability was evaluated using a biotin tracer as described previously [31]. Briefly, after administering pentobarbital sodium (50 mg/kg), the adult mice (8–12 weeks old) were deeply anesthetized and their testes were surgically exposed. A small opening in the tunica albuginea was gently created with fine forceps, and 20 μl of fresh PBS containing 10 mg/ml biotin tracker EZ-Link Sulfo-NHS-LC-Biotin (21335, Thermo Fisher Scientific, Waltham, MA, USA) and 1 mM $CaCl_2$ was carefully injected by a Hamilton syringe into the interstitium of testes, with attention to not inject too far into the testes to avoid disrupting the intra-tubular compartment. Then, the testes were incubated in NHS-linked biotin for 30 min at RT. After incubation in the tracer, the testes were fixed in 4% PFA overnight at RT and processed for cryosection. Cryosections (5 μm thick) were stained with Alexa Fluor 488-conjugated streptavidin (S11223, Thermo Fisher) and photographed under a confocal microscope (Leica, Germany).

Terminal deoxynucleotidyl transferase dUTP nick end labeling staining assay

P7, P14, and P60 testes from Ctrl and Hnrnpc cKO mice ($n = 4$ mice per genotype) were fixed in 4% PFA overnight and then were gradient dehydrated in sucrose and embedded in OCT. The samples were cut into 5 μm cryosections and stored at –80°C. Terminal deoxynucleotidyl transferase dUTP nick end labeling (TUNEL) staining was performed using an In Situ Cell Death Detection Kit, Fluorescein (11684795910, Roche, USA), according to the manufacturer's instructions. The images were captured under a confocal microscope (Leica, Germany).

Ribonucleic acid-sequencing analysis

The total RNA of SCs was extracted from testes of five to six mice at P14 or six to eight mice at P56 for each replicate using TRIzol reagents (15596026, Invitrogen, USA). Two biological replicates were used for RNA-seq. 2 μg total RNAs of purified SCs at P14 and P56 were used for stranded RNA-seq library preparation using a KC-Digital Stranded mRNA Library Prep Kit for Illumina (DR08502, Wuhan Seqhealth Co Ltd, China). The kit eliminates the duplication bias during PCR and sequencing steps by using a unique molecular identifier of eight random bases to label the pre-amplified cDNA molecules. The library products corresponding to 200–500 bps were enriched and sequenced on Novaseq 6000 sequencer (Illumina) with a PE150 model. Raw sequencing data was filtered with the Trimmomatic program (version 0.36). Sequences were mapped to the UCSC MM10 mouse genome using STAR software (version 2.5.3a). Reads mapped to the exon regions of each gene were counted by featureCounts (Subread-1.5.1; Bioconductor) and then reads per kilobase per million was calculated. Genes differentially expressed between groups were identified using the edgeR package (version 3.12.1). A p-value cut-off of 0.05 and a fold-change cut-off of two were used to judge the statistical significance. Gene ontology (GO) analysis and Kyoto encyclopedia of genes and genomes (KEGG) enrichment analysis for genes with differentially expressed were performed using KOBAS software (version: 2.1.1) with a P-value cut-off of 0.05 to judge statistically significant enrichment.

Statistical analysis

All experiments were performed independently in triplicate, and all data were presented as mean ± SD. Statistical analysis was performed by one-way analysis of variance or the student t-test using the SPSS17.0 software. When $p < 0.05$, the difference between groups was considered significant. P-values are denoted in figures by $^{*}p < 0.05$, $^{**}p < 0.01$, and $^{***}p < 0.001$; *ns*, not significant.

Results

Heterogeneous nuclear ribonucleoprotein C encodes a highly conserved protein in mouse testes

Multialignment and phylogenetic analyses of hnRNPC orthologs in eight vertebrate species by Protein BLAST online (https://blast.ncbi.nlm.nih.gov/Blast.cgi) revealed that hnRNPC was highly conserved during evolution (Supplementary Figure S1A and B), suggesting a conserved role of hnRNPC. To figure out its role, we firstly analyzed the expression of hnRNPC protein in various mouse organs by Western blot, and the results showed that hnRNPC was ubiquitously expressed in multiple organs yet predominantly in the testes (Supplementary Figure S1C and D). We also determined hnRNPC expression in developmental testes, and the data showed that hnRNPC was highly expressed from P7 (postnatal day 7) to P42 (Figure 1A and Supplementary Figure S2A and B). The results of IHC revealed that hnRNPC

was expressed in the nuclei of pachytene spermatocytes (PS, black triangle), round spermatids (RS, green triangle), and SCs (red triangle) (Figure 1B). Together, these data show that hnRNPC is highly conserved and expressed in the nuclei of testicular cells.

Heterogeneous nuclear ribonucleoprotein C in Sertoli cells is essential for male fertility in mice

Given the high expression of hnRNPC in SCs, we speculate that hnRNPC in SCs may play a role in spermatogenesis. To test this hypothesis, we generated *Hnrnpc* cKO mice (also named cKO) by mating *Hnrnpc* $^{flox/flox}$ mice with the *Amh*-Cre mice. *Amh-Cre*–mediated recombination results in the deletion of exons 4–5 and a null allele of *Hnrnpc* in SCs (Supplementary Figure S2C). Compared with Ctrls, the mRNA expression level of *Hnrnpc* was significantly reduced in *Hnrnpc* cKO testes (Figure 1C), and the protein levels of hnRNPC were almost absent in purified SCs from cKO mice (Figure 1D and Supplementary Figure S2D and E). Furthermore, co-staining of hnRNPC with sex determining region Y-box 8 (SOX8, an SC marker) in adult Ctrl and cKO testis sections further confirmed a specific ablation of hnRNPC in the *Hnrnpc* cKO SCs at both P56 and P3 mice (Figure 1E and Supplementary Figure S2F). These data suggest that the *Hnrnpc* gene was successfully inactivated in SCs in the *Hnrnpc* cKO male mice.

To investigate whether hnRNPC deficiency in SCs could affect male fertility, we conducted a fertility test using *Hnrnpc* cKO males bred with fertility–proven WT females for 4 months. Yet, no pups were produced, suggesting that the *Hnrnpc* cKO males were completely sterile (Figure 1F). In addition, the adult testis size of *Hnrnpc* cKO mice was grossly smaller than Ctrl littermates (Figure 1G), and the total number of spermatozoa in cauda epididymis was also markedly reduced in *Hnrnpc* cKO mice compared with Ctrls (Figure 1H). Growth analysis revealed that there was no significant difference between the body weight of Ctrl and *Hnrnpc* cKO mice along with time (Supplementary Figure S3A); yet, the testis weight was obviously reduced from P14 (Supplementary Figure S3B). Meanwhile, compared with Ctrls, the ratio of testis weight/body weight of *Hnrnpc* cKO mice was significantly reduced starting from P14 (Figure 1I). PAS staining revealed that all stages of the seminiferous epithelial cycle could be found in the testis of adult Ctrl mice, whereas some vacuoles were observed in the testis of *Hnrnpc* cKO mice, as indicated by asterisks (Figure 1J and Supplementary Figure S3C). Statistical analysis also showed that the tubular diameters in P120 *Hnrnpc* cKO testes were much smaller than that in Ctrls (Supplementary Figure S3D). Furthermore, few mature spermatozoa could be found in the *Hnrnpc* cKO epididymis (Figure 1J). Together, these results prove that hnRNPC in SCs is necessary for spermatogenesis and male fertility in mice.

Ablation of heterogeneous nuclear ribonucleoprotein C in Sertoli cells results in defects of germ cell development

To explore the underlying molecular reasons for the infertility caused by hnRNPC depletion in SCs, we first examined the GC development by the IF staining of the GC marker DDX4. The results showed that the average number of DDX4-positive cells per seminiferous tubule was significantly decreased in *Hnrnpc* cKO testes compared to Ctrl testes at P60 (Figure 2A and B and Supplementary Figure S4A). Consistent with this result, the TUNEL assay revealed significantly increased apoptotic cells per seminiferous tubule in *Hnrnpc* cKO testes at P60 compared with Ctrls (Figure 2C and D and Supplementary Figure S4B). Further PAS staining of seminiferous tubules at various stages from Ctrl and *Hnrnpc* cKO mice revealed a dramatically reduced number of elongating/elongated spermatids (ESs) and abnormal head shaping occurred in *Hnrnpc* cKO testes, which indicates that ablation of hnRNPC in SCs causes defects in spermiogenesis (Figure 2E and F). In addition, stepwise analysis of spermatids within testes showed that the deformed sperm head was observed from step 10 spermatids in *Hnrnpc* cKO mice (Figure 2G), suggesting that the sperm formation and nuclei condense were affected in *Hnrnpc* cKO mice. We also analyzed the specific markers of SPG (*Gfra1*, *Zbtb16*), preleptotene (PL) spermatocyte (*Hormad1*, *Sycp3*), pachytene spermatocyte (PS) (*Spag6*, *Tbp1*), RS (*Tssk1*, *Acrv1*), and ES (*Prm1*, *Tnp1*) to further determine the GC types and their relative quantity in adult testes (P60). The results showed that the expression of markers of SPG were significantly upregulated, while that of meiotic or postmeiotic cells markers, especially RS and ES markers, were significantly decreased (Figure 2H), which was consistent with the results of PAS. Together, these observations indicate that ablation of hnRNPC in SCs causes more apoptosis, and defects in spermiogenesis, thus leading to significant GC loss.

Proliferation of Sertoli cells was affected in *Hnrnpc* cKO testes

Since the maintenance of the number of SCs contributes to the function of SCs during spermatogenesis, we first analyzed the number of SCs by immunostaining of WT1, known as an SC marker, in Ctrl and *Hnrnpc* cKO testes. As shown in Figure 3A and B, the number of WT1-positive cells per seminiferous tubule was significantly decreased in *Hnrnpc* cKO testis compared to Ctrl testis from P5 to P21. To better understand why the number of SCs was reduced in *Hnrnpc* cKO testes, we performed dual IF staining for GATA binding protein 4 (GATA4; a marker of immature SCs; red) and Ki67 (a marker of proliferation; green) at P3, P5, and P7 testes to examine the proliferation of SCs. The results showed that in the *Hnrnpc* cKO mouse testes, the numbers of proliferating SCs (Ki67$^+$ and GATA4$^+$) were significantly less than the Ctrls at P3 and P5 (Figure 3C and D). In addition, we assessed the proliferative potential in purified SCs from the Ctrl and *Hnrnpc* cKO mice at P3 and P5 using EdU labeling, as the incorporation of the thymidine analog EdU into nuclear DNA provides a reliable measure of S-phase entry in fixed cells. The percentage of EdU-positive (proliferating) SCs in *Hnrnpc* cKO mice at P3 and P5 was significantly lower than in the Ctrls (Figure 3E and F). Immature SCs continue to proliferate until 12–17 days postpartum, we then also detected the apoptosis of SCs in P7 and P14 testes. Although almost no apoptosis in SCs was observed in Ctrl and cKO testes at P7 (Supplementary Figure S4C and D) and P14 (Supplementary Figure S4E and F), the number of SCs was significantly decreased in adult cKO testes (Supplementary Figure S5A and B). Together, these outcomes suggest that hnRNPC is essential for regulating cell proliferation in SCs.

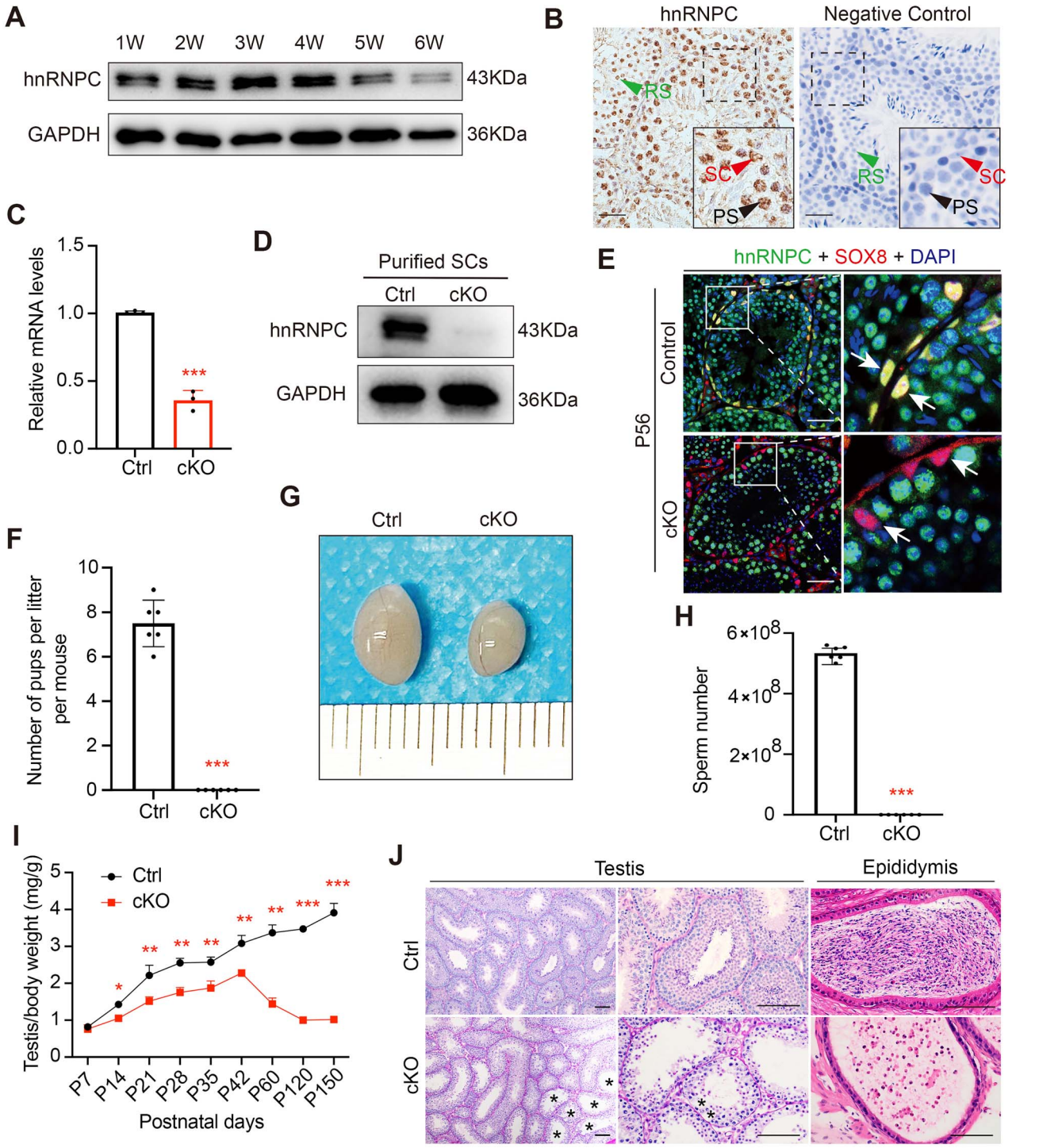

Figure 1. Deficiency of hnRNPC in SCs impairs spermatogenesis. (A) hnRNPC expression of WT testes at different developmental stages, including postnatal day 1 week (1 W), 2 W, 3 W, 4 W, 5 W, and 6 W, was measured by Western blotting. GAPDH was used as loading Ctrl. (B) IHC staining of hnRNPC in adult WT testes at postnatal day 42 (P42) is shown (*left*). The image on the right shows negative Ctrl. Dashed boxes showed the localization of the enlarged images (PS: pachytene spermatocyte; RS: round spermatid). IgG as a negative Ctrl. Scale bars = 20 μm. (C) RT-qPCR was conducted to test the expression of the *Hnrnpc* mRNA in the testes of the Ctrl and *Hnrnpc* cKO (cKO) mice. Data are presented as mean ± SD; $n = 3$; $^{***}p < 0.001$ by Student *t*-test. (D) Western blot analysis of hnRNPC protein level in the SCs of the Ctrl and cKO mice at P42. GAPDH served as a loading Ctrl. (E) Representative co-IF images of hnRNPC and SOX8 in Ctrl and cKO testis sections at P56 are shown. Scale bars = 50 μm. (F) The average number of pups per litter from adult Ctrl and cKO male mice are shown. Data are presented as mean ± SD; $n = 6$; $^{***}p < 0.001$ by Student *t*-test. (G) Gross morphology of testes from adult Ctrl and cKO male mice are shown. (H) Sperm counts analysis in caudal epididymis. Data are presented as mean ± SEM; $n = 6$; $^{***}p < 0.001$ by Student *t*-test. (I) Testis growth curves of the Ctrl and cKO mice testes from postnatal P7–P150. Data are presented as mean ± SD; $n = 3$; $^{*}p < 0.05$, $^{**}p < 0.01$, and $^{***}p < 0.001$ by Student *t*-test. (J) PAS staining shows the histology of the Ctrl and cKO testis (*left*) and epididymis (*right*) sections at P56. Vacuoles (labeled by asterisks) was observed in the seminiferous tubules of cKO mice. Scale bars = 100 μm.

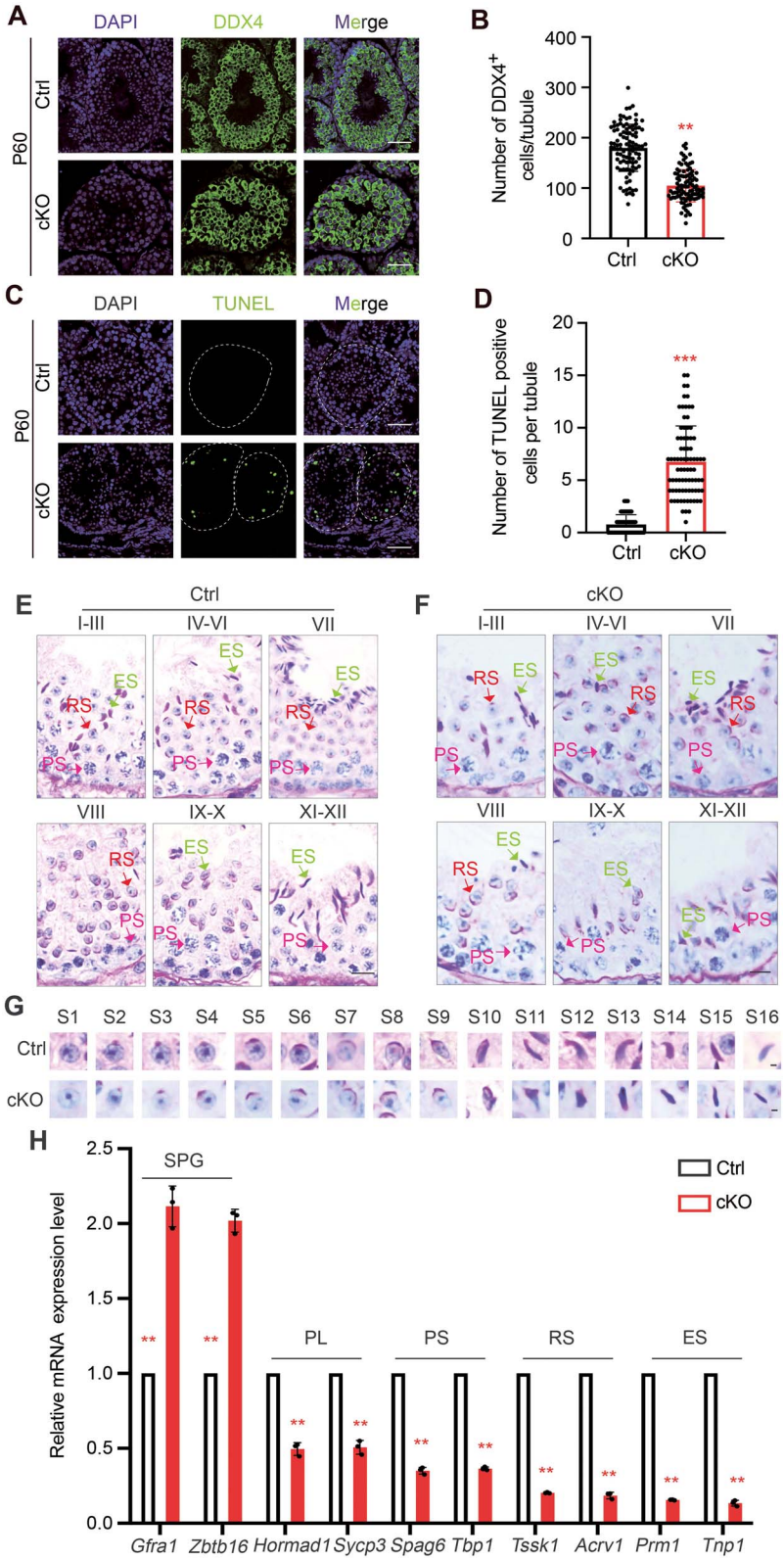

Figure 2. Aberrant spermiogenesis was detected in *Hnrnpc* cKO mice. (A) Co-IF staining for GC marker (DDX4) in cross-sections of testes at P60 from the Ctrl and cKO mice. Nuclei were stained with DAPI. Scale bars = 50 μm. (B) Histogram showing the average number of DDX4-positive GCs per seminiferous tubule in (A). Data are presented as mean ± SD; $n = 100$; $^{**}p < 0.01$ by Student *t*-test. (C) Representative images of the apoptosis of GCs in Ctrl and cKO testes at P56 were determined by TUNEL staining. Scale bars = 50 μm. (D) Histogram shows the average number of TUNEL-positive cells per seminiferous tubule. Data are presented as mean ± SD; $n = 80$; $^{**}p < 0.01$ by Student *t*-test. (E–F) Histological analyses of different stages of testicular sections from Ctrl and cKO mice are shown. PS: pachytene spermatocyte; RS: round spermatid; ES: elongating/elongated spermatid; scale bars = 20 μm. (G) Spermatids in different stages of acrosome development in Ctrl and cKO mice were detected by PAS staining. Scale bars = 1 μm. (H) RT-qPCR analysis of mRNA expression in Ctrl and cKO mice testis at P60, *Gapdh* was used as normalized Ctrl. Data was shown as mean ± SD; $n = 3$; $^{**}p < 0.01$ by Student *t*-test; SPG: spermatogonia; PL: preleptotene spermatocyte; PS: pachytene spermatocyte; RS: round spermatid; ES: elongating/elongated spermatid.

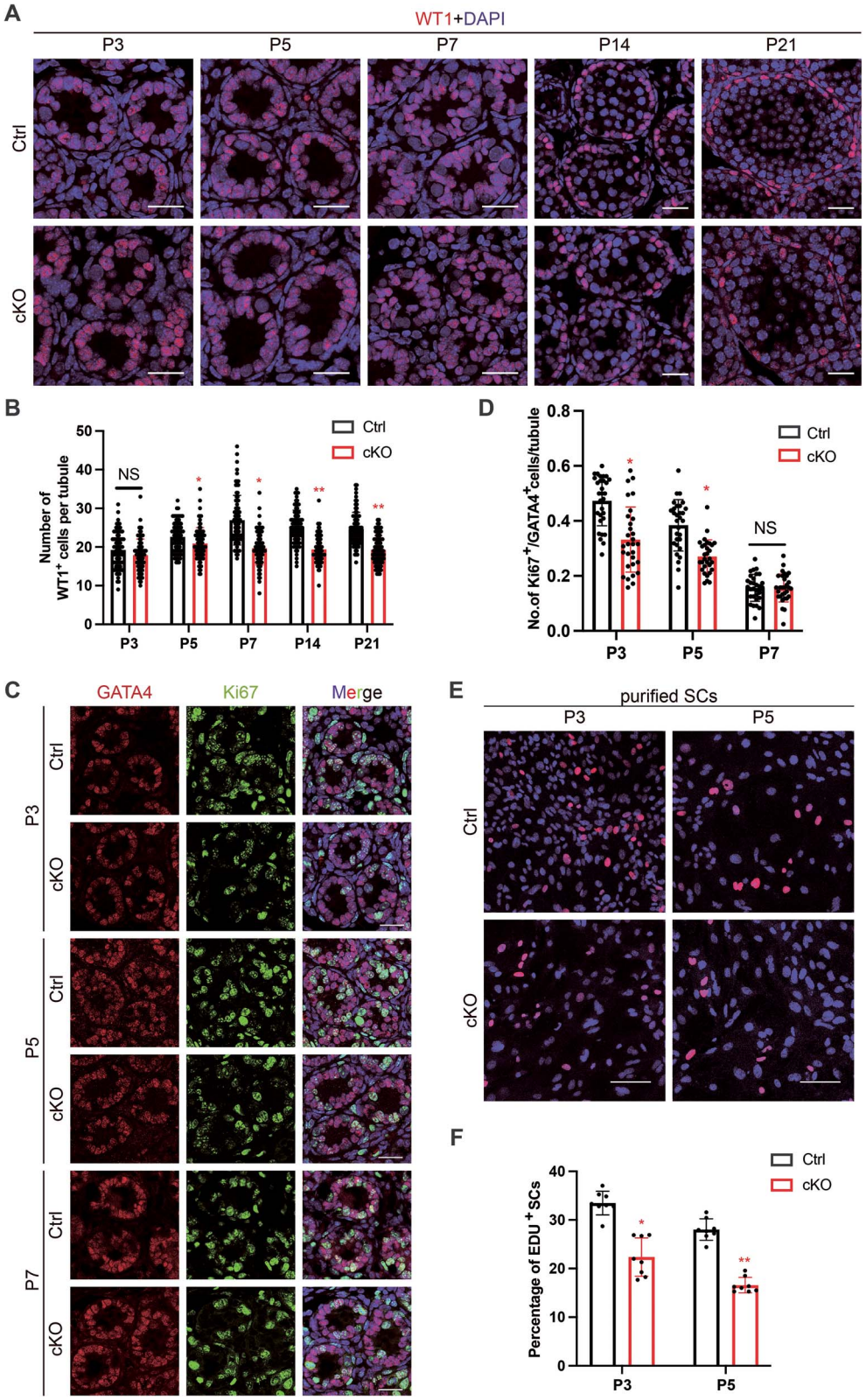

Figure 3. Ablation of hnRNPC in SCs exhibits abnormal cell proliferation. (A) Images show WT1 and DAPI nuclear dye staining at various ages of Ctrl and cKO testes. Scale bars = 50 μm. (B) Quantification of WT1$^+$ SCs per tubule in the transverse section of the testes in (A). Data are presented as mean ± SD. $n = 3$ mice. For each mouse was randomly checked to count. $^*p < 0.05$ and $^{**}p < 0.01$ by Student t-test. (C) Representative images of double IF staining for Ki67 and GATA4 in Ctrl and cKO testes at P3, P5, and P7 are shown. Scale bars = 50 μm. (D) The histogram shows the quantification of the ratio of Ki67$^+$ cells to WT1$^+$ cells per tubule in (C). Data are presented as mean ± SD; $n = 3$ mice; $^*p < 0.05$ by Student t-test; NS, not significant. (E) Representative images of IF staining of EdU in primary SCs isolated from Ctrl and cKO testes at P3 and P5 are shown. Scale bars = 50 μm. (F) Histograms show the quantification of the percentage of EdU$^+$ SCs in (E). Data are presented as mean ± SD; $n = 8$; $^*p < 0.05$ and $^{**}p < 0.01$ by Student t-test.

Heterogeneous nuclear ribonucleoprotein C deficiency in Sertoli cells results in the disorganization of the actin cytoskeleton of Sertoli cells

Cytoskeletal proteins play an important role in cell shape, motility, as well as maintenance of cell junctions, which help to keep normal epithelial morphology and function, and serve as the foundation for the integrity of the BTB and its dynamic restructuring [32]. To further analyze the effects of hnRNPC depletion on SCs, IF staining of actin filamentous (F-ACTIN; a marker for ES, red) was performed to assess if the cytoskeletal structure was disorganized in adult *Hnrnpc* cKO SCs. Peanut agglutinin (PNA; green) was used to label acrosome of spermatids and discern different stages of seminiferous tubules. In Ctrl adult testes, F-ACTIN was organized in the apical ES around the SC-spermatid interface (Figure 4A; white arrowheads) and the basal ES at the SC–SC interface near the basement membrane (Figure 4A; white arrows). However, in the seminiferous epithelium of adult *Hnrnpc* cKO mice, the F-ACTIN network was significantly disrupted since the expression of F-ACTIN was no longer organized at the basal ES to support BTB function. Instead, it was diffuse, extensive, or branched (stages VII–VIII) spread in the adluminal compartment (Figure 4A; yellow arrows). Since SCs have an extensive network of microtubules arranged in a spoke-like pattern required for GC migration, we then measured the length of spoke-like pattern in β-ACTIN and α-TUBULIN in the cross sections of seminiferous tubules. In *Hnrnpc* cKO testes, a significantly shorter length of β-ACTIN (Figure 4B and C) and α-TUBULIN (Figure 4D and E) was observed, and the microtubular arrangement did not assume the spoke-like pattern, suggesting that organized ACTIN and microtubular arrangement was disrupted in *Hnrnpc* cKO mouse testes. In addition, in purified SCs from Ctrl mice, the typical F-ACTIN filaments were stretched across the SC cytosol in an organized and arranged fashion. However, actin filaments were extensively truncated and misorganized in purified SCs of *Hnrnpc* cKO mice, appearing as considerably branched filaments (Figure 4F). These findings indicate that the cytoskeletal organization of SCs was disrupted in hnRNPC-deficient SCs.

Inactivation of heterogeneous nuclear ribonucleoprotein C in Sertoli cells disrupted the blood–testis barrier integrity

Since the disorganized cytoskeleton in SCs could disrupt their polarity, which might further affect the function of BTB, we then assessed the integrity of the BTB with a biotin-tracing assay. In the Ctrl testis, biotin tracer signals (green) were found only in the testicular interstitium and the basal compartment of the seminiferous tubules in the Ctrl testis, and no signal was observed in the tubular lumen. In contrast, the biotin tracer penetrated the adluminal compartment and diffused throughout almost all of the seminiferous tubules in the *Hnrnpc* cKO testes (Figure 5A and B). Images with lower magnification were provided in Supplementary Figure S5C and D.

As it has already been confirmed that the cytoskeletal proteins are involved in maintaining BTB function [33], we also examined the expression of BTB-associated proteins by IF staining to verify the dysfunction of BTB integrity. Compared with Ctrl mouse testes, the distribution of the basal ES proteins at the basement membrane in the seminiferous tubules, including N-cadherin (Figure 5C and D and Supplementary Figure S5E) and β-catenin (Figure 5E and F and Supplementary Figure S5F), was dramatically altered in *Hnrnpc* cKO mouse testes. IF signals corresponding to N-cadherin were diffusely located and extended away from the site, which were obviously enhanced, but β-catenin signals were significantly decreased (Figure 5C–F). In addition, the expression of Connexin-43, known as a predominant GA protein, was also evidently decreased in *Hnrnpc* cKO mouse testes compared with Ctrls (Figure 5G and H and Supplementary Figure S5G). As shown in Figure 5I and J and Supplementary Figure S5H, the total length of vimentin filaments (a cytoskeleton protein) was considerably shortened in *Hnrnpc* cKO seminiferous tubules compared with Ctrls. Consistent with IF staining analyses, results of the Western blot experiment of BTB-associated proteins, including Vimentin, β-catenin, and Connexin-43, also confirmed decreased expression levels in *Hnrnpc* cKO testes (Figure 5K and L and Supplementary Figure S6A–D). Together, these results indicate that the hnRNPC in SCs is required to maintain BTB integrity.

Heterogeneous nuclear ribonucleoprotein regulates gene transcriptomes in Sertoli cells

To elucidate the underlying gene regulatory network of hnRNPC in SCs, we purified SCs from P14 and P56 Ctrl and *Hnrnpc* cKO mice and compared the transcriptomes via deep RNA-seq. Genes with 2-fold changes in expression level were classified as DEGs. Compared to the Ctrl SCs, in *Hnrnpc* cKO SCs at P14, 115 and 357 genes were upregulated and downregulated, respectively (Figure 6A and Supplementary Table S3), with the downregulated genes being enriched in the regulation of the actin cytoskeleton and cell adhesion molecules as revealed by KEGG analysis (Figure 6B), which was consistent with the disorganization of actin cytoskeletons of SCs observed in *Hnrnpc* cKO mice. In *Hnrnpc* cKO SCs at P56, 409 genes were upregulated, and 302 genes were downregulated, respectively (Figure 6C and Supplementary Table S4), with the downregulated genes enriched in TJ (Figure 6D), which might explain why the BTB was disrupted in adult *Hnrnpc* cKO testes. Considering the common regulated genes might be very important in SCs function, the overlapped DEGs between P14 and P56 were analyzed. Overall, 92 overlapped DEGs were identified, accounting for 19.5% and 12.9% of the total DEGs of *Hnrnpc* cKO SCs, respectively (Figure 6E). GO analysis revealed that most of the DEGs were related to functions including cell adhesion, regulation of cell proliferation, apoptotic process regulation, and male gonad development (Figure 6F), which also correlated well with the impaired proliferative ability of SCs after hnRNPC ablation. In addition, a total of 85 downregulated DEGs overlapped between P14 and P56, and most were related to functions including SC development and male gonad development (Figure 6G and H).

Next, we selected 10 downregulated and three upregulated genes to validate their expression using RT-qPCR. The expression of these selected genes shared the same trend as RNA-seq (Supplementary Figure S7A and B), suggesting the results of RNA-seq were reliable. Notably, among those downregulated genes, *Jakmip1* (also known as *Marlin1*) was associated with gamma-aminobutyric acid receptors and the microtubule cytoskeleton [34], and *Hsd17b1* [35] participated in head shape formation. Extended synaptotagmin-like protein 3 (*Esyt3*) [36], Clusterin (*Clu*) [37], and doublesex and mab-3 related transcription factor 1 (*Dmrt1*) [38], *Tulp2* were all involved in spermatogenesis.

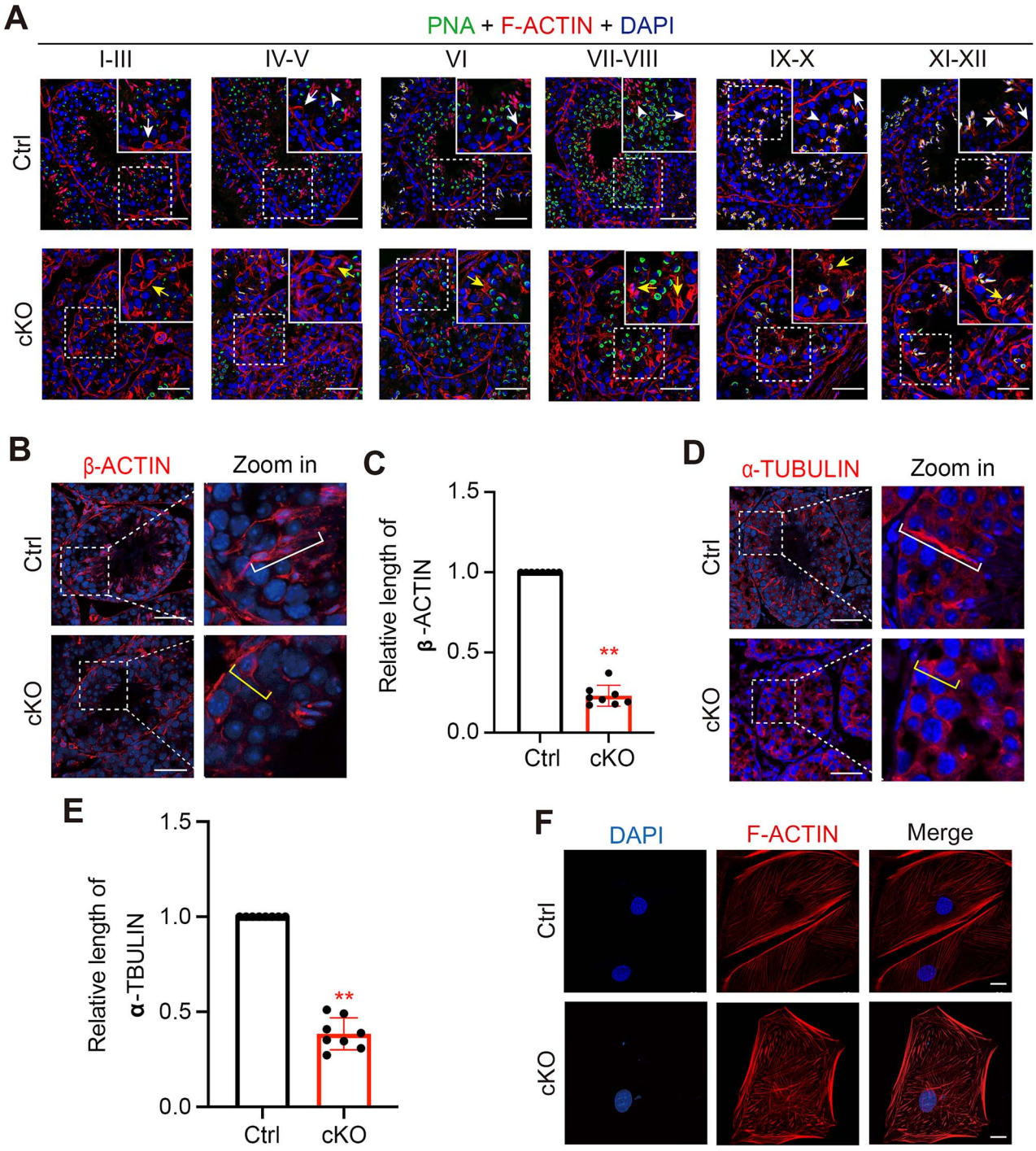

Figure 4. Deletion of hnRNPC in SCs disrupts the cytoskeletal structure of SCs. (A) Representative images of IF staining with PNA and F-ACTIN on different stages of testis sections from Ctrl and cKO mice at P60 are shown. Nuclei were stained with DAPI. Scale bars = 50 μm. The boxed region in each image is enlarged in the upper right corner. Arrows and arrowheads in Ctrl indicated basal ES and apical ES, respectively. Ectopically expressed F-ACTIN in *Hnrnpc* cKO testes was indicated by arrows. Scale bars = 50 μm. (B) Representative images of IF staining of β-ACTIN with DAPI nuclear counterstain on the testis sections from Ctrl and cKO mice at P60 are shown. Scale bars = 50 μm. (C) The histogram shows relative length of the β-ACTIN in (B). The relative length of the β-ACTIN indicates the ratio of β-ACTIN signals reaching from the basal membrane up to the tubular lumen in β-ACTIN-stained cKO testicular sections to WT testicular sections. Data are presented as mean ± SD; $n = 8$; $^{**}p < 0.01$ by Student t-test. (D) Representative images of IF staining of α-TUBULIN with DAPI nuclear counterstain on the testis sections from Ctrl and cKO mice at P60 are shown. Scale bars = 50 μm. (E) The histogram shows relative length of the α-TUBULIN in (D). The relative length of the α-TUBULIN indicates the ratio of β-ACTIN signals reaching from the basal membrane up to the tubular lumen in α-TUBULIN-stained cKO testicular sections to WT testicular sections. Data are presented as mean ± SD; $n = 8$; $^{**}p < 0.01$ by Student t-test. (F) Representative images of the F-ACTIN filaments in primary SCs isolated from Ctrl and cKO mice are shown. Scale bars = 10 μm.

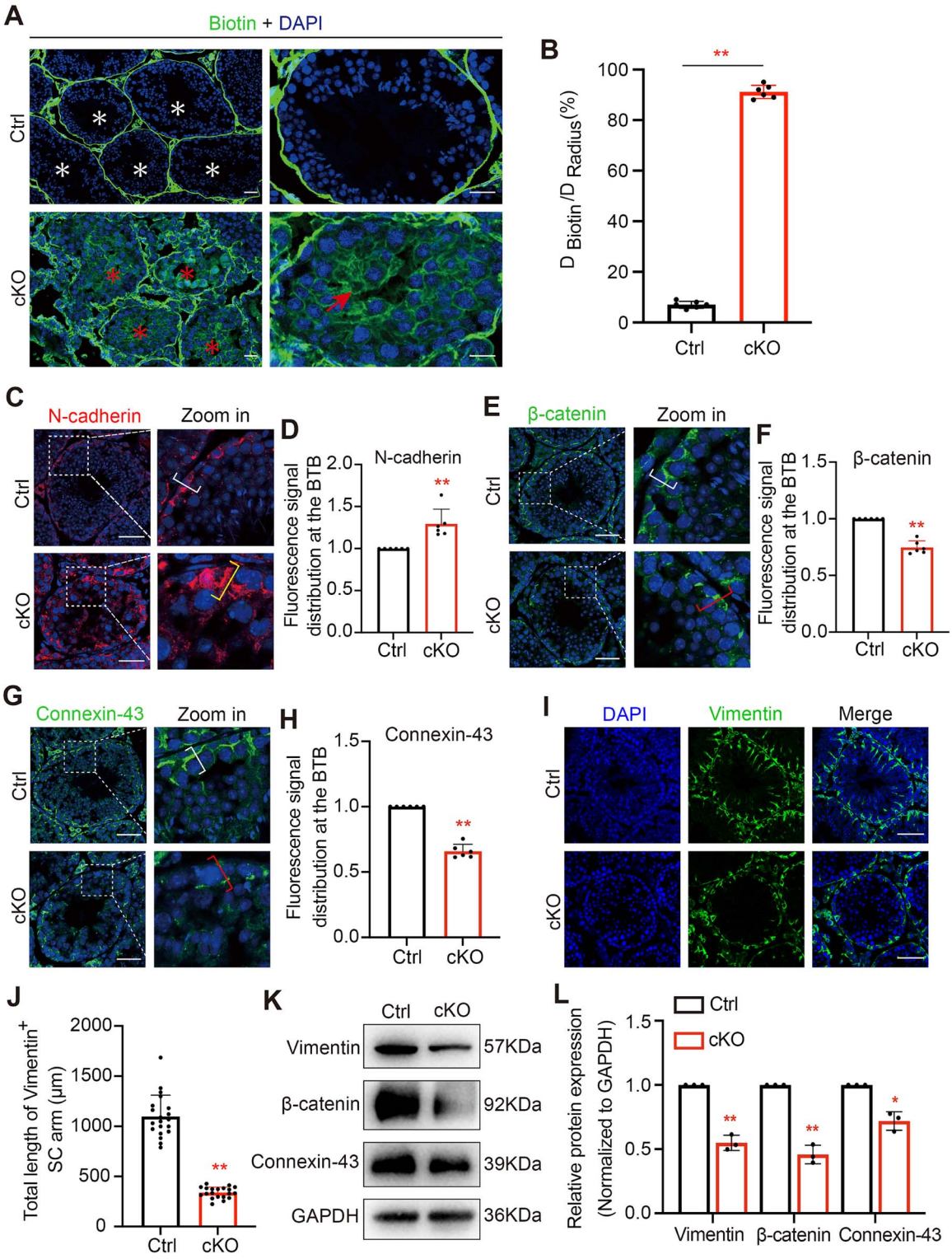

Figure 5. hnRNPC-deficient SCs displayed the disruption of BTB integrity. (A) Biotin signal was limited to the testicular interstitium and the basal compartment of the seminiferous tubules in Ctrl mice (annotated by asterisks). In contrast, a strong biotin signal was observed in the lumen of seminiferous tubules of cKO testes (annotated by asterisks and arrow). Scale bars = 50 μm. (B) Histogram showing the quantification of fluorescence distance traveled by biotin tracker vs the tubule radius for $n = 5$ mice in each group; $^{**}p < 0.01$ by unpaired Student t-test. (C–H) IF staining of basal ES proteins N-cadherin (C), β-catenin (E) and GA protein Connexin 43 (G) in Ctrl testes and cKO testes at P60, and the histograms summarized results of fluorescence images regarding changes in the relative distribution of N-cadherin (D), β-catenin (F), Connexin 43 (H) in in Ctrl and cKO testes. Scale bars = 50 μm. Data are presented as mean ± SD; $n = 6$; $^{**}p < 0.01$ by Student t-test. (I) Representative IF staining images of cytoskeletal protein Vimentin in Ctrl and cKO testis sections at P60 are shown. Scale bars = 50 μm. (J) The histogram shows the quantification of total length of the Vimentin-positive SC arm in (I). Data are presented as mean ± SD; $n = 20$; $^{**}p < 0.01$ by Student t-test. (K) Western blotting shows the altered expression of BTB-associated proteins in purified SCs from Ctrl and cKO mouse testes at P60. GAPDH served as a loading Ctrl. (L) The histogram shows the quantification of BTB-associated protein levels in (K). Data are presented as mean ± SD; $n = 3$; $^{*}p < 0.05$ and $^{**}p < 0.01$ by Student t-test.

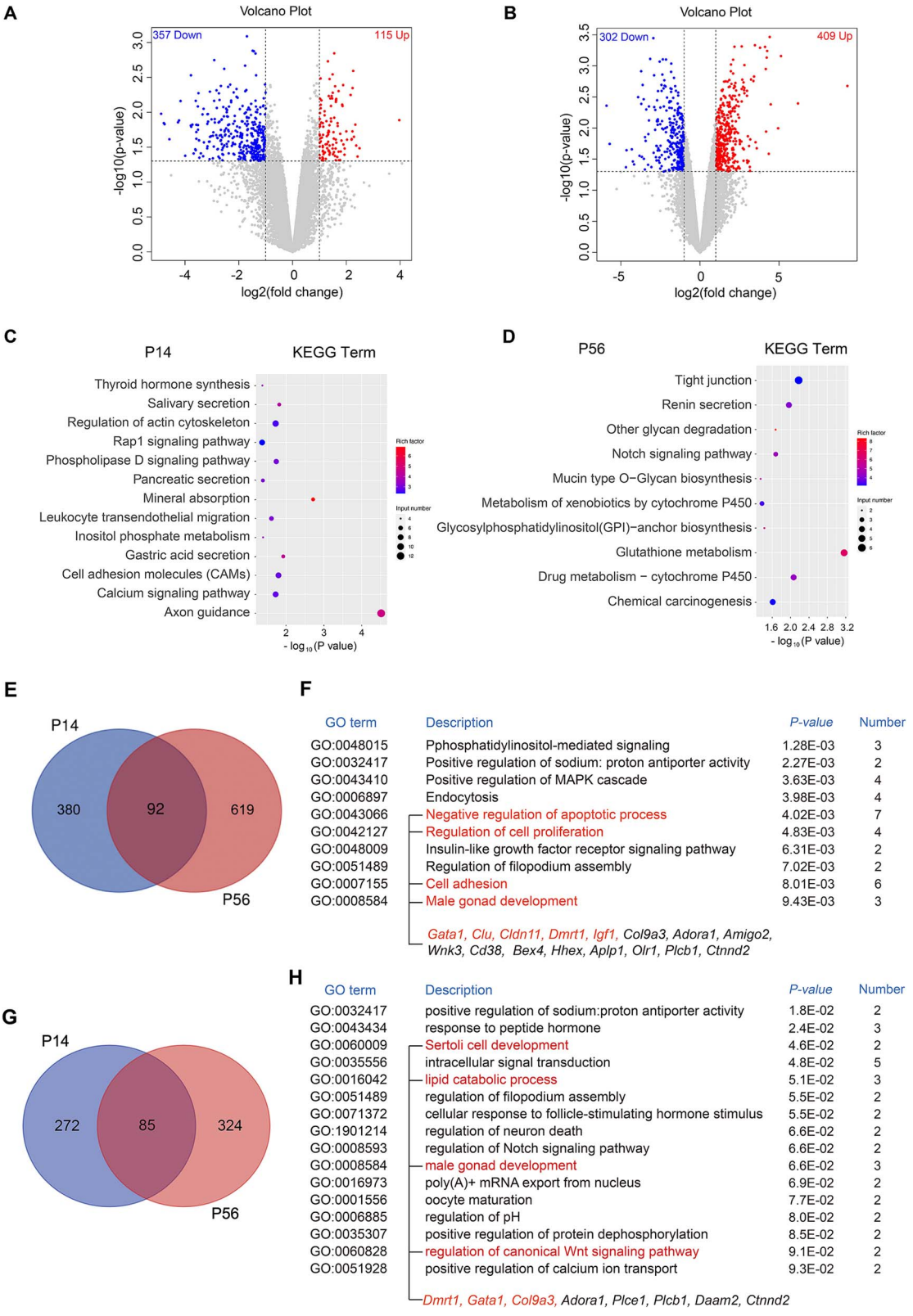

GO term	Description	*P-value*	Number
GO:0048015	Pphosphatidylinositol-mediated signaling	1.28E-03	3
GO:0032417	Positive regulation of sodium: proton antiporter activity	2.27E-03	2
GO:0043410	Positive regulation of MAPK cascade	3.63E-03	4
GO:0006897	Endocytosis	3.98E-03	4
GO:0043066	Negative regulation of apoptotic process	4.02E-03	7
GO:0042127	Regulation of cell proliferation	4.83E-03	4
GO:0048009	Insulin-like growth factor receptor signaling pathway	6.31E-03	2
GO:0051489	Regulation of filopodium assembly	7.02E-03	2
GO:0007155	Cell adhesion	8.01E-03	6
GO:0008584	Male gonad development	9.43E-03	3

Gata1, Clu, Cldn11, Dmrt1, Igf1, Col9a3, Adora1, Amigo2, Wnk3, Cd38, Bex4, Hhex, Aplp1, Olr1, Plcb1, Ctnnd2

GO term	Description	*P-value*	Number
GO:0032417	positive regulation of sodium:proton antiporter activity	1.8E-02	2
GO:0043434	response to peptide hormone	2.4E-02	3
GO:0060009	Sertoli cell development	4.6E-02	2
GO:0035556	intracellular signal transduction	4.8E-02	5
GO:0016042	lipid catabolic process	5.1E-02	3
GO:0051489	regulation of filopodium assembly	5.5E-02	2
GO:0071372	cellular response to follicle-stimulating hormone stimulus	5.5E-02	2
GO:1901214	regulation of neuron death	6.6E-02	2
GO:0008593	regulation of Notch signaling pathway	6.6E-02	2
GO:0008584	male gonad development	6.6E-02	3
GO:0016973	poly(A)+ mRNA export from nucleus	6.9E-02	2
GO:0001556	oocyte maturation	7.7E-02	2
GO:0006885	regulation of pH	8.0E-02	2
GO:0035307	positive regulation of protein dephosphorylation	8.5E-02	2
GO:0060828	regulation of canonical Wnt signaling pathway	9.1E-02	2
GO:0051928	positive regulation of calcium ion transport	9.3E-02	2

Dmrt1, Gata1, Col9a3, Adora1, Plce1, Plcb1, Daam2, Ctnnd2

Figure 6. Heterogeneous nuclear ribonucleoprotein deficiency induces genome-wide transcriptome profile alterations in SCs. (A) Volcano plot showing the distribution of DEGs in the purified SCs from Ctrl and cKO mice at P14. The dots represent significantly downregulated and upregulated genes, (fold change ≥ 2, and FDR ≤ 0.05), were shown. (B) KEGG enrichment analysis of the downregulated genes at P14. (C) Volcano plot showing the distribution of DEGs in the purified SCs from Ctrl and cKO mice at P56. (D) KEGG enrichment analysis of the downregulated genes at P56. (E) The Venn diagram shows overlapping of 92 common DEGs at two developmental time points, P14 and P56. (F) GO term analyses of total DEGs in primary SCs of cKO mice are shown. The top 10 enriched GO pathways in the DEGs of P14 and P56 were illustrated by gene counts and *p*-values. (G) The Venn diagram shows overlapping of 85 common downregulated genes at two developmental time points, P14 and P56. (H) GO term analyses of downregulated genes in primary SCs of cKO mice are shown. The top 16 enriched GO pathways in the downregulated genes of P14 and P56 were illustrated by gene counts and *p*-values.

We also examined downregulated and upregulated genes validated in P56 SCs by RT-qPCR in testes, whose changes were almost identical to those in P56 SCs (Supplementary Figure S7C–F). Reduced expression of androgen receptor (AR)-regulated genes in purified SCs compared to testes was also observed in both Ctrl and *Hnrnpc* cKO mice, such as *Ccnd1, Rhox5*, and *Sox9* (Supplementary Figure S7G and H), suggesting reduced AR signaling on SCs after culturing the purified SCs. Taken together, the dysregulation of the aforementioned genes involved in cytoskeletal organization and spermatogenesis in *Hnrnpc* cKO SCs likely caused the disruption of BTB integrity in *Hnrnpc* cKO mice.

Discussion

The results of this study revealed that hnRNPC deficiency in SCs resulted in compromised proliferation of SCs as well as remarkable GCs loss, and the mutant mice were completely infertile. Furthermore, cytoskeletal organization and cell polarity of SCs and BTB integrity were found to be significantly disrupted in *Hnrnpc* cKO mouse testes. Transcriptomic analysis indicated that the SC-specific deficiency of hnRNPC caused the downregulation of genes involved in cell adhesion, cell proliferation, and apoptotic process regulation, supporting that hnRNPC in SCs is essential for maintaining normal gene regulation during spermatogenesis.

AMH-Cre begins to express Cre recombinase in SCs at around E11.5, the time of SC specification [39]. Consistent with this, hnRNPC deletion in SCs had early effects on SCs in P3 testes, and the proliferative capacity of SCs was reduced, which may account for the reduced tubular diameters and average number of DDX4-positive cells per seminiferous tubule in adult *Hnrnpc* cKO testes. The above effect together with the apoptosis of GCs, synergistically caused a reduction in total GC output as well as the testis weight in *Hnrnpc* cKO mice. The number of SCs in adult cKO testes was also significantly reduced, resulting much smaller adult testes with smaller tubular diameters. Apart from the reduced proliferative capacity, the function of SCs was also significantly altered after hnRNPC deletion, as characterized by the disruption of SC polarity as well as the integrity of the BTB. The BTB is structurally composed of TJs, GAs, and basal ES between adjacent SCs in the seminiferous epithelium. Nevertheless, the ultrastructure of the BTB may undergo dynamic restructuring during stages VIII–XI to allow the transit and entry of PL spermatocytes into the adluminal compartment, ensuring the proper progression of subsequent meiosis and spermiogenesis [40]. This probably explains why the mRNA levels of PL spermatocytes and later GCs were significantly reduced in adult cKO testes.

A previous study reported that F-ACTIN was involved in spermatogenesis [41]; in this study, we also found that the dispersed localization of F-ACTIN and disruption of microtubular arrangement, which may partially explain the loss of elongated sperm observed in our *Hnrnpc* cKO testis, as the cytoarchitecture may be compromised and unable to maintain and keep chained GCs to the spermatogonial epithelium. In addition, in our *Hnrnpc* cKO mice, BTB integrity was significantly impaired and the expression of the BTB-associated proteins (e.g., such as β-Catenin and Connexin43) was also considerably reduced. The abnormal expression of actin and junction proteins caused by *Hnrnpc* deletion may reduce the association of actin with TJ and ES proteins, which may further disrupt the dynamic reconstruction of the apical ES and tubulobulbar complex at the interface between SCs and spermatids, which is essential for spermiogenesis [40]. As a result, spermiogenesis was severely impaired, the number of elongating and ESs was significantly reduced in the seminiferous tubules, and ultimately few spermatozoa were observed in the epididymis of *Hnrnpc* cKO mice.

Data from RNA-seq demonstrated that the deletion of hnRNPC in SCs could cause downregulation of genes related to cell adhesion, regulation of cell proliferation, apoptotic process regulation, and male gonad development. Among these genes, *Tulp2* was reported to play an essential function in maintaining the production of ESs and the regulation of events related to the cytoskeleton and apoptosis [42]. Furthermore, it has been proved that multiple roles of DMRT1 are involved in regulating the differentiation of juvenile testes, including postnatal differentiation of SCs and GCs [43]. Hakkarainen et al. conducted a study involving the *Hsd17b1* knockout of male mice and noticed that the cell junctions between SCs and GCs were disrupted, and the head shape of elongating spermatids displayed significant defects in spermatogenesis sometimes [44]. Compared with Ctrls, these genes (*Tulp2, Jakmip1, Sh3gl3, Hsd17b1*, and *Dmrt1*) are significantly downregulated in *Hnrnpc* cKO SCs, which was consistent with the phenotypic defects observed in *Hnrnpc* cKO mice at the molecular level. However, it remains unknown whether the expression of these genes was regulated by hnRNPC directly or indirectly, which needs to be further investigated in future related experiments.

Nevertheless, it is equally important to acknowledge the limitations of this research. Firstly, our study mainly focused on the function of hnRNPC in SCs during spermatogenesis and demonstrated that the hnRNPC is essential for BTB integrity and the maintenance of adult steady-state spermatogenesis. However, whether hnRNPC in GCs also plays an important function in spermatogenesis is still unknown and remains to be clarified. Secondly, as the commercially available antibodies could not be used well for immunoprecipitation or RNA immunoprecipitation assays, the direct target genes bound and regulated by hnRNPC that are involved in disrupted cytoskeletal structure, BTB integrity, and spermatogenic defects in *Hnrnpc* cKO SCs need to be further investigated. We recognize that further investigations regarding the detailed mechanism of hnRNPC in the regulation of spermatogenesis are still needed.

In summary, the current study demonstrates an essential role of hnRNPC within SCs during GC development, which provides robust evidence and expands our understanding of the role of the hnRNPs family in spermatogenesis and contributes to further investigation of the distinct functions of SCs supporting the maintenance of spermatogenesis.

Supplementary data

Supplementary data are available at *BIOLRE* online.

Author contributions

YG and SY conceived this study and supervised the project. SM, GS, CC, MW, JY, JY, and QM performed histological analysis, IF staining, and

all animal work. CC performed data analysis. JY and MX performed RT-qPCR analysis. SM wrote the manuscript. QM and SY revised the manuscript.

Conflict of interest: The authors have declared that no conflict of interest exists.

Data availability

The RNA-seq original dataset is deposited in the NCBI SRA (Sequence Read Achieve) database with the accession number PRJNA1025315.

References

1. Clermont Y. Kinetics of spermatogenesis in mammals: seminiferous epithelium cycle and spermatogonial renewal. *Physiol Rev* 1972; **52**:198–236.
2. Griswold MD. Spermatogenesis: the commitment to meiosis. *Physiol Rev* 2016; **96**:1–17.
3. Ezeh UI. Beyond the clinical classification of azoospermia: opinion. *Hum Reprod* 2000; **15**:2356–2359.
4. Gao Y, Xiao X, Lui WY, Lee WM, Mruk D, Cheng CY. Cell polarity proteins and spermatogenesis. *Semin Cell Dev Biol* 2016; **59**:62–70.
5. Lui WY, Lee WM, Cheng CY. Transforming growth factor-beta3 perturbs the inter-Sertoli tight junction permeability barrier in vitro possibly mediated via its effects on occludin, zonula occludens-1, and claudin-11. *Endocrinology* 2001; **142**:1865–1877.
6. Li JC, Mruk D, Cheng CY. The inter-Sertoli tight junction permeability barrier is regulated by the interplay of protein phosphatases and kinases: an in vitro study. *J Androl* 2001; **22**:847–856.
7. Franca LR, Hess RA, Dufour JM, Hofmann MC, Griswold MD. The Sertoli cell: one hundred fifty years of beauty and plasticity. *Andrology* 2016; **4**:189–212.
8. Tan IP, Roy C, Sáez JC, Sáez CG, Paul DL, Risley MS. Regulated assembly of connexin33 and connexin43 into rat Sertoli cell gap junctions. *Biol Reprod* 1996; **54**:1300–1310.
9. Risley MS, Tan IP, Roy C, Saez JC. Cell-, age- and stage-dependent distribution of connexin43 gap junctions in testes. *J Cell Sci* 1992; **103**:81–96.
10. Boyer A, Girard M, Thimmanahalli DS, Levasseur A, Céleste C, Paquet M, Duggavathi R, Boerboom D. mTOR regulates gap junction Alpha-1 protein trafficking in Sertoli cells and is required for the maintenance of spermatogenesis in mice. *Biol Reprod* 2016; **95**:13.
11. Bertoldo MJ, Guibert E, Faure M, Guillou F, Ramé C, Nadal-Desbarats L, Foretz M, Viollet B, Dupont J, Froment P. Specific deletion of AMP-activated protein kinase (α1AMPK) in mouse Sertoli cells modifies germ cell quality. *Mol Cell Endocrinol* 2016; **423**:96–112.
12. Dreyfuss G, Matunis MJ, Pinol-Roma S, Burd CG. hnRNP proteins and the biogenesis of mRNA. *Annu Rev Biochem* 1993; **62**: 289–321.
13. Nakielny S, Dreyfuss G. The hnRNP C proteins contain a nuclear retention sequence that can override nuclear export signals. *J Cell Biol* 1996; **134**:1365–1373.
14. Shetty S. Regulation of urokinase receptor mRNA stability by hnRNP C in lung epithelial cells. *Mol Cell Biochem* 2005; **272**: 107–118.
15. Zhang J, Cho SJ, Shu L, Yan W, Guerrero T, Kent M, Skorupski K, Chen H, Chen X. Translational repression of p53 by RNPC1, a p53 target overexpressed in lymphomas. *Genes Dev* 2011; **25**: 1528–1543.
16. Ehrmann I, Dalgliesh C, Tsaousi A, Paronetto MP, Heinrich B, Kist R, Cairns P, Li W, Mueller C, Jackson M, Peters H, Nayernia K, *et al.* Haploinsufficiency of the germ cell-specific nuclear RNA binding protein hnRNP G-T prevents functional spermatogenesis in the mouse. *Hum Mol Genet* 2008; **17**:2803–2818.
17. Li JP, Guo WB, Li F, He JC, Yu QF, Wu XQ, Li JM, Mao XM. HnRNPL as a key factor in spermatogenesis: lesson from functional proteomic studies of azoospermia patients with sertoli cell only syndrome. *J Proteomics* 2012; **75**:2879–2891.
18. Xu H, Guo J, Wu W, Han Q, Huang Y, Wang Y, Li C, Cheng X, Zhang P, Xu Y. Deletion of Hnrnpk gene causes infertility in male mice by disrupting spermatogenesis. *Cells* 2022; **11**:11.
19. Wen Y, Ma X, Wang X, Wang F, Dong J, Wu Y, Lv C, Liu K, Zhang Y, Zhang Z, Yuan S. hnRNPU in Sertoli cells cooperates with WT1 and is essential for testicular development by modulating transcriptional factors Sox8/9. *Theranostics* 2021; **11**:10030–10046.
20. Feng S, Li J, Wen H, Liu K, Gui Y, Wen Y, Wang X, Yuan S. hnRNPH1 recruits PTBP2 and SRSF3 to modulate alternative splicing in germ cells. *Nat Commun* 2022; **13**:3588.
21. Wang XL, Li JM, Yuan SQ. Characterization of the protein expression and localization of hnRNP family members during murine spermatogenesis. *Asian J Androl* 2023; **25**:314–321.
22. Wang X, Fan X, Zhang J, Wang F, Chen J, Wen Y, Wang L, Li T, Li H, Gu H, Zhang Y, Yuan S. hnRNPA2B1 represses the disassembly of arsenite-induced stress granules and is essential for male fertility. *Cell Rep* 2024; **43**:113769.
23. Feng S, Wen H, Liu K, Xiong M, Li J, Gui Y, Lv C, Zhang J, Ma X, Wang X, Yuan S. hnRNPH1 establishes Sertoli-germ cell crosstalk through cooperation with PTBP1 and AR, and is essential for male fertility in mice. *Development* 2023; **150**:150.
24. Christian KJ, Lang MA, Raffalli-Mathieu F. Interaction of heterogeneous nuclear ribonucleoprotein C1/C2 with a novel cis-regulatory element within p53 mRNA as a response to cytostatic drug treatment. *Mol Pharmacol* 2008; **73**:1558–1567.
25. Merrill BM, Barnett SF, WM LS, Williams KR. Primary structure differences between proteins C1 and C2 of HeLa 40S nuclear ribonucleoprotein particles. *Nucleic Acids Res* 1989; **17**: 8441–8449.
26. Yang N, Liu L, Liu X, Chen Y, Lu J, Wang Z. hnRNPC promotes malignancy in pancreatic cancer through stabilization of IQGAP3. *Biomed Res Int* 2022; **2022**:1–17.
27. Sun W, Xing B, Sun Y, Du X, Lu M, Hao C, Lu Z, Mi W, Wu S, Wei H, Gao X, Zhu Y, *et al.* Proteome analysis of hepatocellular carcinoma by two-dimensional difference gel electrophoresis: novel protein markers in hepatocellular carcinoma tissues. *Mol Cell Proteomics* 2007; **6**:1798–1808.
28. Wu Y, Zhao W, Liu Y, Tan X, Li X, Zou Q, Xiao Z, Xu H, Wang Y, Yang X. Function of HNRNPC in breast cancer cells by controlling the dsRNA-induced interferon response. *EMBO J* 2018; **37**:e99017.
29. Williamson DJ, Banik-Maiti S, DeGregori J, Ruley HE. hnRNP C is required for postimplantation mouse development but is dispensable for cell viability. *Mol Cell Biol* 2000; **20**:4094–4105.
30. Wu YQ, Duan P, Wen YJ, Zhang J, Wang XL, Dong J, Zhao Q, Feng SL, Lv CY, Guo Y, Namekawa SH, Yuan SQ. UHRF1 establishes crosstalk between somatic and germ cells in male reproduction. *Cell Death Dis* 2022; **13**:13.
31. Furuse M, Hata M, Furuse K, Yoshida Y, Haratake A, Sugitani Y, Noda T, Kubo A, Tsukita S. Claudin-based tight junctions are crucial for the mammalian epidermal barrier: a lesson from claudin-1-deficient mice. *J Cell Biol* 2002; **156**:1099–1111.
32. Lie PP, Mruk DD, Lee WM, Cheng CY. Cytoskeletal dynamics and spermatogenesis. *Philos Trans R Soc Lond B Biol Sci* 2010; **365**: 1581–1592.
33. Cui L, Gu Y, Liu S, Li M, Ye J, Zhang F, Luo X, Chang WL, Gui Y. TBC1D20 is essential for mouse blood–testis barrier integrity through maintaining the epithelial phenotype and modulating the maturation of Sertoli cells. *Reprod Sci* 2020; **27**:1443–1454.
34. Vidal RL, Ramírez A, Castro M, Concha II, Couve A. Marlin-1 is expressed in testis and associates to the cytoskeleton and GABAB receptors. *J Cell Biochem* 2008; **103**:886–895.

35. Hakkarainen J, Zhang FP, Jokela H, Mayerhofer A, Behr R, Cisneros-Montalvo S, Nurmio M, Toppari J, Ohlsson C, Kotaja N, Sipilä P, Poutanen M. Hydroxysteroid (17β) dehydrogenase 1 expressed by Sertoli cells contributes to steroid synthesis and is required for male fertility. *FASEB J* 2018; **32**: 3229–3241.
36. Evans E, Hogarth C, Mitchell D, Griswold M. Riding the spermatogenic wave: profiling gene expression within neonatal germ and Sertoli cells during a synchronized initial wave of spermatogenesis in mice. *Biol Reprod* 2014; **90**:90.
37. Riaz MA, Stammler A, Borgers M, Konrad L. Clusterin signals via ApoER2/VLDLR and induces meiosis of male germ cells. *Am J Transl Res* 2017; **9**:1266–1276.
38. Lindeman RE, Murphy MW, Agrimson KS, Gewiss RL, Bardwell VJ, Gearhart MD, Zarkower D. The conserved sex regulator DMRT1 recruits SOX9 in sexual cell fate reprogramming. *Nucleic Acids Res* 2021; **49**:6144–6164.
39. Lécureuil C, Fontaine I, Crepieux P, Guillou F. Sertoli and granulosa cell-specific Cre recombinase activity in transgenic mice. *Genesis* 2002; **33**:114–118.
40. Dong H, Chen Z, Wang C, Xiong Z, Zhao W, Jia C, Lin J, Lin Y, Yuan W, Zhao AZ, Bai X. Rictor regulates spermatogenesis by controlling Sertoli cell cytoskeletal organization and cell polarity in the mouse testis. *Endocrinology* 2015; **156**:4244–4256.
41. Qian X, Mruk DD, Cheng YH, Tang EI, Han D, Lee WM, Wong EW, Cheng CY. Actin binding proteins, spermatid transport and spermiation. *Semin Cell Dev Biol* 2014; **30**: 75–85.
42. Zheng M, Chen X, Cui Y, Li W, Dai H, Yue Q, Zhang H, Zheng Y, Guo X, Zhu H. TULP2, a new RNA-binding protein, is required for mouse spermatid differentiation and male fertility. *Front Cell Dev Biol* 2021; **9**:623738.
43. Kim S, Bardwell VJ, Zarkower D. Cell type-autonomous and non-autonomous requirements for Dmrt1 in postnatal testis differentiation. *Dev Biol* 2007; **307**:314–327.
44. Hakkarainen J, Zhang FP, Jokela H, Mayerhofer A, Behr R, Cisneros-Montalvo S, Nurmio M, Toppari J, Ohlsson C, Kotaja N, Sipilä P, Poutanen M. Hydroxysteroid (17β) dehydrogenase 1 expressed by Sertoli cells contributes to steroid synthesis and is required for male fertility. *FASEB J* 2018; **32**:3229–3241.